A Boundary Element Model for Underwater Acoustics in Shallow Water

J.A.F. Santiago[1], **L.C. Wrobel**[2]

Abstract: This work presents a boundary element formulation for two-dimensional acoustic wave propagation in shallow water. It is assumed that the velocity of sound in water is constant, the free surface is horizontal, and the seabed is irregular. The boundary conditions of the problem are that the sea bottom is rigid and the free surface pressure is atmospheric.

For regions of constant depth, fundamental solutions in the form of infinite series can be employed in order to avoid the discretisation of both the free surface and bottom boundaries. When the seabed topography is irregular, it is necessary to divide the fluid region using the subregions technique. In this case, only irregular bottom boundaries and interfaces between regions of different depth need to be discretised.

Numerical simulations of several problems are included, ranging from smooth to abrupt variations of the seabed. The results are verified by comparison with a more standard BEM formulation in which the complete seabed is discretised and truncated at a large distance.

keyword: Boundary element method, subregions, underwater acoustics, shallow water, waveguides

1 Introduction

Due to the advent of high-speed computers and the recent developments of numerical physics, sound propagation in the ocean can be studied and quantitatively described in greater detail with the more exact wave theory.

Increasing concern for coastal areas has, in recent years, focussed studies of ocean acoustic wave propagation on shallow water environments. The most common numerical techniques used to model underwater acoustic wave propagation are ray methods, normal mode methods, and parabolic equation methods [Jensen, Kuperman, Porter and Schmidt (1994)]. Ray methods are most commonly used in deep water and are restricted to high frequencies; normal mode methods are best suited for low frequencies but experience difficulties with domains that are both range and depth dependent; parabolic equation methods neglect backscattering effects which are likely to be important in very shallow water and near the shore [Grilli, Pedersen and Stepanishen (1998)].

[1] Brunel University, Department of Mechanical Engineering, Uxbridge, Middlesex, UB8 3PH, UK, on leave from COPPE/Federal University of Rio de Janeiro, Department of Civil Engineering, Rio de Janeiro, Brazil

[2] Brunel University, Department of Mechanical Engineering, Uxbridge, Middlesex, UB8 3PH, UK

The present paper proposes a novel boundary element formulation for the numerical modelling of shallow water acoustic propagation, in the frequency domain, over irregular bottom topography. The model assumes a two-dimensional geometry, representative of coastal regions, which have little variation in the long shore direction. A recent application of the boundary element method (BEM) using a hybrid model which combines a standard BEM in an inner region with varying bathimetry and an eigenfunction expansion in the outer region of constant depth was presented by Grilli, Pedersen and Stepanishen (1998). An important earlier work on acoustic scattering in the open ocean was presented by Dawson and Fawcett (1990), in which the waveguide surfaces were taken to be flat except for a compact area of deformation where the acoustic scattering takes place.

The BEM model presented here makes use of two modified Green's functions, one of which satisfies the free surface boundary condition while the other directly satisfies the boundary conditions on the free surface and the horizontal part of the bottom boundary. Alternatively, a Green's function in the form of eigenfunction expansions is employed to improve the convergence characteristics of the latter. Therefore, only bottom irregularities and interfaces need to be discretised.

Results of the propagation and scattering of underwater acoustic waves in a region containing a vertical step-up, in a region of constant depth containing a bottom deformation in the form of a cosine bell, and in a region representative of the seabed close to shore, are included to assess the accuracy of the numerical solutions.

2 Governing Equations of the Problem

Consider the problem of acoustic wave propagation in a region Ω of infinite extent, shown in Fig. 1. Assuming that this medium in the absence of perturbations is quiescent, the velocity of sound is constant and the source of acoustic disturbance is time-harmonic, the problem is governed by the Helmholtz equation [Kinsler, Frey, Coppens and Sanders (1982)]:

$$\nabla^2 u + k^2 u = -\sum_{\alpha=1}^{Nes} B_\alpha \delta\left(\mathbf{E}_\alpha, \mathbf{S}\right) \qquad in\ \Omega \tag{1}$$

where u is the velocity potential, B_α is the magnitude of the acoustic source $\mathbf{E}_\alpha$ located at $(x_{E_\alpha}, y_{E_\alpha})$, $\mathbf{S}$ is the source point located at (x_S, y_S), Nes is the number of acoustic sources, $\delta\left(\mathbf{E}_\alpha, \mathbf{S}\right)$ is the Dirac delta generalised function and $k = w/c$

is the wave number, in which w is the frequency and c is the velocity of sound in water.

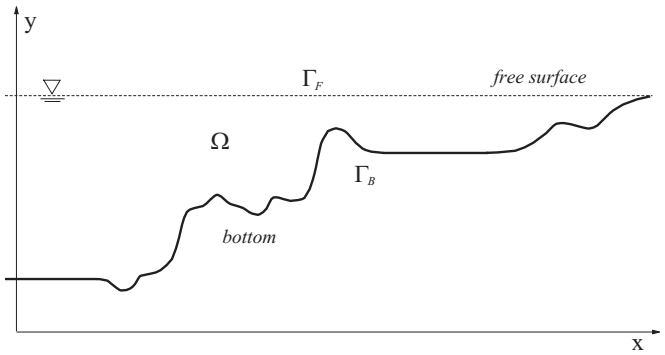

Figure 1 : General ocean section for 2D acoustic propagation problems in shallow water

The problem is subject to the following boundary conditions:

a) Atmospheric pressure at the free surface

$$u(\mathbf{X}) = 0 \qquad on\ \Gamma_F \tag{2}$$

b) Zero penetration velocity at the (rigid) seabed

$$\frac{\partial u}{\partial n}(\mathbf{X}) = 0 \qquad on\ \Gamma_B \tag{3}$$

c) Sommerfeld radiation condition at infinity

$$\frac{\partial u}{\partial n}(\mathbf{X}) = iku(\mathbf{X}) \tag{4}$$

in which Γ_F is the free surface, Γ_B is the irregular bottom, and n is the outward normal vector. According to Green's second identity, Eq. (1) can be transformed into the following boundary integral equation [Chen and Zhou (1992); Lacerda (1997)]

$$C(\mathbf{S})\,u(\mathbf{S}) = \int_\Gamma G(\mathbf{S},\mathbf{X})\frac{\partial u}{\partial n}(\mathbf{X})\,d\Gamma(\mathbf{X}) - \int_\Gamma \frac{\partial G(\mathbf{S},\mathbf{X})}{\partial n(\mathbf{X})}u(\mathbf{X})\,d\Gamma(\mathbf{X}) + \sum_{\alpha=1}^{Nes} B_\alpha G(\mathbf{E}_\alpha,\mathbf{S}) \tag{5}$$

where Γ is equal to $\Gamma_F \cup \Gamma_B$, $\mathbf{X}$ is the field point located at (x,y) and $G(\mathbf{S},\mathbf{X})$ is the free-space Green's function. The functions $u(\mathbf{X})$ and $\partial u/\partial n(\mathbf{X})$ represent the velocity potential and its normal derivative. The coefficient $C(\mathbf{S})$ depends on the boundary geometry at the source point $\mathbf{S}$. It is noted that the Green's function implicitly satisfies the Sommerfeld condition, therefore no discretisation of the boundary at infinity is necessary.

3 Numerical Analysis

3.1 Boundary element method

General propagation problems with irregular seabed topography can be dealt with by the subregions technique [Santiago, Telles and Valentim (1999)]. In this case the domain Ω is divided into several regions, as depicted in Fig. 2. Two types of subregions can be seen in the figure, for which different fundamental solutions are employed. In the first (Ω_2 and Ω_4) the region has irregular bottom while in the other (Ω_1 and Ω_3) it has a constant depth.

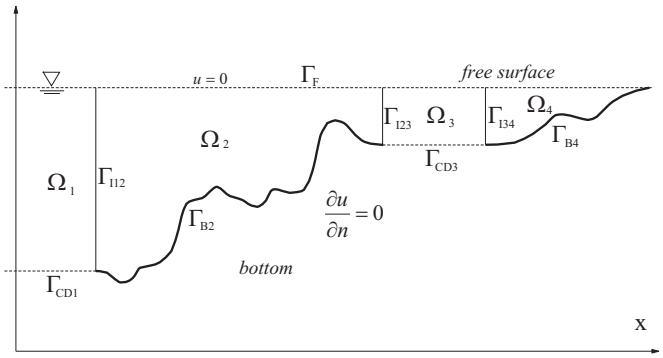

Figure 2 : Regions dividing a typical shallow water section

Instead of using the fundamental solution of the Helmholtz equation for the free-space, Green's functions which directly satisfy the boundary conditions either on Γ_F or on Γ_F, Γ_{CD1} and Γ_{CD3} are adopted. Therefore, only the irregular parts of the bottom boundaries (Γ_{B2} and Γ_{B4}) and interfaces (Γ_{I12}, Γ_{I23} and Γ_{I34}) need to be discretised.

Introducing the appropriate boundary conditions into Eq. (5) yields the following integral equation for a region Ω_χ with irregular bottom:

$$C(\mathbf{S})\,u(\mathbf{S}) = -\int_{\Gamma_{B\chi}} \frac{\partial G_f(\mathbf{S},\mathbf{X})}{\partial n(\mathbf{X})}u(\mathbf{X})\,d\Gamma(\mathbf{X}) + \int_{\Gamma_I}\left[G_f(\mathbf{S},\mathbf{X})\frac{\partial u}{\partial n}(\mathbf{X}) - \frac{\partial G_f(\mathbf{S},\mathbf{X})}{\partial n(\mathbf{X})}u(\mathbf{X})\right]d\Gamma(\mathbf{X}) + \sum_{\alpha=1}^{Nes_\chi} B_\alpha G_f(\mathbf{E}_\alpha,\mathbf{S}) \tag{6}$$

and for a region Ω_χ with constant depth:

$$C(\mathbf{S})\,u(\mathbf{S}) = \int_{\Gamma_I}\left[G_D(\mathbf{S},\mathbf{X})\frac{\partial u}{\partial n}(\mathbf{X}) - \frac{\partial G_D(\mathbf{S},\mathbf{X})}{\partial n(\mathbf{X})}u(\mathbf{X})\right]d\Gamma(\mathbf{X}) + \sum_{\alpha=1}^{Nes_\chi} B_\alpha G_D(\mathbf{E}_\alpha,\mathbf{S}) \tag{7}$$

where Nes_χ is the number of acoustic sources in the region Ω_χ, $\Gamma_{B\chi}$ is the specific irregular bottom and Γ_I is the union of all interfaces, taking into account the direction of integration, belonging to region Ω_χ.

In order to solve Eq. (6) and (7) numerically, the external boundary and interfaces are discretised into a number of el-

ements whose geometries are modelled through shape functions and geometrical nodal points. Over these elements, the velocity potential and its normal derivative are interpolated as functions of the element nodal points. Constant elements with linear geometry have been used in this work.

Applying the collocation method to Eq. (6) and (7) gives, in terms of an intrinsic coordinate η, for a region Ω_χ with irregular bottom:

$$C(\mathbf{S}_p)\,u(\mathbf{S}_p) = -\sum_{q=1}^{Neb_\chi} u_q \frac{L_q}{2}\int_{-1}^{+1}\frac{\partial G_f(\mathbf{S}_p,\mathbf{X}_q)}{\partial n(\mathbf{X}_q)}d\eta + \sum_{q=1}^{Nei_\chi}\frac{L_q}{2}\left[v_q\int_{-1}^{+1}G_f(\mathbf{S}_p,\mathbf{X}_q)\,d\eta - u_q\int_{-1}^{+1}\frac{\partial G_f(\mathbf{S}_p,\mathbf{X}_q)}{\partial n(\mathbf{X}_q)}d\eta\right] + \sum_{\alpha=1}^{Nes_\chi} B_\alpha G_f(\mathbf{E}_\alpha,\mathbf{S}_p) \tag{8}$$

and for a region Ω_χ with constant depth:

$$C(\mathbf{S}_p)\,u(\mathbf{S}_p) = \sum_{q=1}^{Nei_\chi}\frac{L_q}{2}\left[v_q\int_{-1}^{+1}G_D(\mathbf{S}_p,\mathbf{X}_q)\,d\eta - u_q\int_{-1}^{+1}\frac{\partial G_D(\mathbf{S}_p,\mathbf{X}_q)}{\partial n}d\eta\right] + \sum_{\alpha=1}^{Nes_\chi} B_\alpha G_D(\mathbf{E}_\alpha,\mathbf{S}_p) \tag{9}$$

where p ranges from 1 to Nf_χ, with Nf_χ the total number of functional nodes, Neb_χ, Nei_χ are the number of external boundary elements and the number of elements of all interfaces in the region Ω_χ,respectively; $\mathbf{S}_p$ are collocation points and L_q is the length of element Γ_q. Finally, u_q and v_q are the velocity potential and its normal derivative, respectively, at the point $\mathbf{X}_q$ which is the mid-point of element Γ_q.

In the above equations, the first modified Green's function $G_f(\mathbf{S}_p,\mathbf{X}_q)$ identically satisfies the boundary condition on the free surface Γ_F while the second function $G_D(\mathbf{S}_p,\mathbf{X}_q)$ identically satisfies the boundary condition on the free surface Γ_F and seabed Γ_B.

Eq. (8) and (9) are computed for each specific region separately, and are then coupled by imposing continuity of velocity potential and its normal derivative over the interfaces. Hence, applying these equations to all functional nodal points and considering that all boundary conditions are implicitly satisfied leads to

$$\mathbf{Ay} = \mathbf{b} \tag{10}$$

where the system matrix **A** contains the influence coefficients, vector **b** contains the contribution of the acoustic sources, and vector **y** contains the unknown values of velocity potentials **u** at the irregular bottom boundaries, and velocity potentials **u** and their normal derivatives **v** at the interfaces.

3.2 Fundamental solutions

The fundamental solutions mentioned in the previous section can be developed by two different means. The first is the method of images using either a single source point reflection or multiple source point reflections, while the second uses eigenfunctions (normal modes) of the depth-separated Helmholtz equation [Jensen, Kuperman, Porter and Schmidt (1994)].

3.2.1 Irregular bottom

For the first subregion type (see Fig. 2) the modified Green's function $G_f(\mathbf{S},\mathbf{X})$, obtained by means of the method of images with a single source, is employed in the following form:

$$G_f(\mathbf{S},\mathbf{X}) = \frac{i}{4}\left[H_0^{(1)}(kr) - H_0^{(1)}\left(kr^{(1F)}\right)\right] \tag{11}$$

$$\frac{\partial G_f(\mathbf{S},\mathbf{X})}{\partial n(\mathbf{X})} = -\frac{ik}{4}\left[H_1^{(1)}(kr)\frac{\partial r}{\partial n} - H_1^{(1)}\left(kr^{(1F)}\right)\frac{\partial r^{(1F)}}{\partial n}\right] \tag{12}$$

where $H_0^{(1)}(\ )$ and $H_1^{(1)}(\ )$ are Hankel functions of the first kind of order 0 and 1, respectively, r and $r^{(1F)}$ are the distances from the field point **X** to the source point **S** and its reflection with respect to the free surface, respectively. These distances can be written as:

$$r = |\mathbf{X}-\mathbf{S}| = \sqrt{(x-x_S)^2+(y-y_S)^2} \qquad \mathbf{X} = (x,y) \qquad \mathbf{S} = (x_S,y_S) \tag{13}$$

$$r^{(1F)} = \left|\mathbf{X}-\mathbf{S}^{(1F)}\right| = \sqrt{(x-x_S)^2+\left(y-y_S^{(1F)}\right)^2} \qquad \mathbf{S}^{(1F)} = \left(x_S, y_S^{(1F)}\right) \tag{14}$$

in which

$$y_S^{(1F)} = 2y_F - y_S \tag{15}$$

where y_F is the y-coordinate of the free surface.

3.2.2 Constant depth

For the second subregion type, the function $G_D(\mathbf{S},\mathbf{X})$ is used in the form of two infinite series, the modified Greens' function $G_F(\mathbf{S},\mathbf{X})$ or $G_B(\mathbf{S},\mathbf{X})$ and the Greens' function $G_m(\mathbf{S},\mathbf{X})$.

The first series, obtained through the method of images with multiple source point reflections, is given by [Jensen, Kuperman, Porter and Schmidt (1994); Santiago and Wrobel

(1999a)]:

$$G_F(\mathbf{S},\mathbf{X}) = \frac{i}{4}\left[H_0^{(1)}(kr) - H_0^{(1)}\left(kr^{(1F)}\right)\right] + \frac{i}{4}\sum_{m=1}^{\infty}(-1)^{m+1}\sum_{j=1}^{2}(-1)^{j+1}\left[H_0^{(1)}\left(kr_m^{(2jF)}\right) - H_0^{(1)}\left(kr_m^{((2j+1)F)}\right)\right] \quad (16)$$

$$G_B(\mathbf{S},\mathbf{X}) = \frac{i}{4}\left[H_0^{(1)}(kr) + H_0^{(1)}\left(kr^{(1B)}\right)\right] + \frac{i}{4}\sum_{m=1}^{\infty}(-1)^{m}\sum_{j=2}^{5}H_0^{(1)}\left(kr_m^{(jB)}\right) \quad (17)$$

with normal derivative:

$$\frac{\partial G_F(\mathbf{S},\mathbf{X})}{\partial n} = -\frac{ik}{4}\left[H_1^{(1)}(kr)\frac{\partial r}{\partial n} - H_1^{(1)}\left(kr^{(1F)}\right)\frac{\partial r^{(1F)}}{\partial n}\right] - \frac{ik}{4}\sum_{m=1}^{\infty}(-1)^{m+1}\sum_{j=1}^{2}(-1)^{j+1}\left[H_1^{(1)}\left(kr_m^{(2jF)}\right)\frac{\partial r_m^{(2jF)}}{\partial n} - H_1^{(1)}\left(kr_m^{((2j+1)F)}\right)\frac{\partial r_m^{((2j+1)F)}}{\partial n}\right] \quad (18)$$

$$\frac{\partial G_B(\mathbf{S},\mathbf{X})}{\partial n} = -\frac{ik}{4}\left[H_1^{(1)}(kr)\frac{\partial r}{\partial n} + H_1^{(1)}\left(kr^{(1B)}\right)\frac{\partial r^{(1B)}}{\partial n}\right] - \frac{ik}{4}\sum_{m=1}^{\infty}(-1)^{m}\sum_{j=2}^{5}H_1^{(1)}\left(kr_m^{(jB)}\right)\frac{\partial r_m^{(jB)}}{\partial n} \quad (19)$$

where the superindices $(1F)$, $(2jF)$, $((2j+1)F)$, $(1B)$ and (jB) identify the reflected source points.

The above expressions (16) and (17) represent the same infinite series of Hankel functions and their images, and only differ in the way the series are truncated. The modified Green's function $G_F(\mathbf{S},\mathbf{X})$ exactly satisfies the boundary condition on the free surface, but its normal derivative produces a very small non-zero value at the bottom boundary. Alternatively, the modified Green's function $G_B(\mathbf{S},\mathbf{X})$ produces a very small residual at the free surface but its normal derivative exactly satisfies the boundary condition at the bottom.

The distances from the field point $\mathbf{X}$ to the reflections of source point $\mathbf{S}$ (see Fig. 3) with respect to free surface(F) and bottom(B) are denoted as $r^{(1F)}$, $r_m^{(2jF)}$ and $r_m^{((2j+1)F)}$ for $G_F(\mathbf{S},\mathbf{X})$ and $r^{(1B)}$ and $r_m^{(2jB)}$ for $G_B(\mathbf{S},\mathbf{X})$ [Santiago and Wrobel (1999b)]. The distances $r_m^{(2jF)}$ and $r_m^{((2j+1)F)}$ can be written as:

$$r_m^{(JF)} = \left|\mathbf{X} - \mathbf{S}^{(JF)}\right| = \sqrt{(x-x_S)^2 + \left(y - y_{S_m}^{(JF)}\right)^2}$$

$$\mathbf{S}^{(JF)} = \left(x_S, y_{S_m}^{(JF)}\right) \quad (20)$$

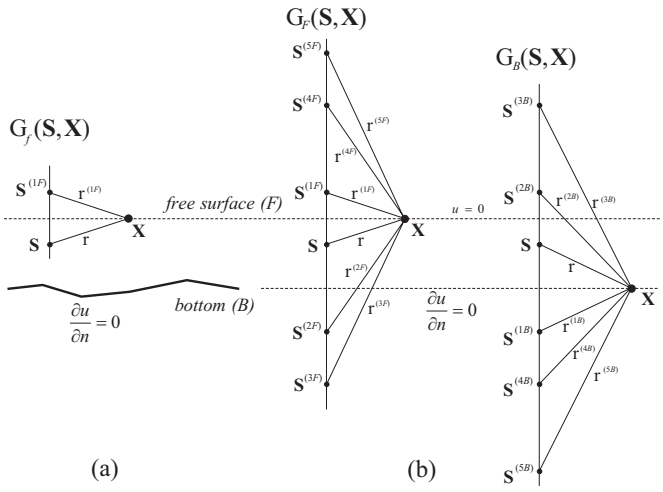

Figure 3 : Distance from field point $\mathbf{X}$ to source point $\mathbf{S}$ and its reflections with respect to free surface and bottom

in which J ranges from 2 to 5, and

$$y_{S_m}^{(2F)} = -2(m-1)y_F + 2my_B - y_S \quad (21)$$

$$y_{S_m}^{(3F)} = 2m(-y_F + y_B) + y_S \quad (22)$$

$$y_{S_m}^{(4F)} = 2m(y_F - y_B) + y_S \quad (23)$$

$$y_{S_m}^{(5F)} = 2(m+1)y_F - 2my_B - y_S \quad (24)$$

where y_B is the y-coordinate of the bottom. Eq. (14), (15) and (20) to (24) are also used for $G_B(\mathbf{S},\mathbf{X})$, with the indices F replaced by B, and vice-versa.

The second series, in terms of normal modes, may be expressed as [Jensen, Kuperman, Porter and Schmidt (1994); Pedersen (1996)]:

$$G_m = \frac{i}{H}\sum_{m=1}^{\infty}\sin\left[k_{ym}(y_F - y_S)\right]\sin\left[k_{ym}(y_F - y)\right]\times \frac{e^{ik_{xm}|x-x_S|}}{k_{xm}} \quad (25)$$

Its derivatives with respect to x and y are:

$$\frac{\partial G_m}{\partial x} = -\frac{|x-x_S|}{H(x-x_S)}\sum_{m=1}^{\infty}\sin\left[k_{ym}(y_F - y_S)\right]\times \sin\left[k_{ym}(y_F - y)\right]e^{ik_{xm}|x-x_S|} \quad (26)$$

$$\frac{\partial G_m}{\partial y} = -\frac{i}{H}\sum_{m=1}^{\infty}\frac{k_{ym}}{k_{xm}}\sin\left[k_{ym}(y_F - y_S)\right]\times \cos\left[k_{ym}(y_F - y)\right]e^{ik_{xm}|x-x_S|} \quad (27)$$

where H is the depth. The parameters k_{xm} and k_{ym} are horizon-

tal and vertical wavenumbers, respectively:

$$k_{ym} = \left(m - \frac{1}{2}\right)\frac{\pi}{H} \tag{28}$$

$$k_{xm} = \sqrt{k^2 - k_{ym}^2} \tag{29}$$

3.2.3 Remarks

A recent paper by Linton (1998) acknowledges that standard representations of the Green's function in terms of infinite sums of images, such as in (16) and (17), usually contain series which converge very slowly, and so are unsuitable for numerical work. The calculation of the Green's function G_m given by (25) can be done much more efficiently due to the exponential term in the series. It is clear that when k_{xm} becomes an imaginary number, *i.e.* when k_{ym} is greater than k, the power of the exponential in (25) becomes real and negative, and the series will decrease very rapidly for $|x - x_S| > 0$. Nevertheless, when coordinate x of the source and field points is the same, *i.e.* $x - x_S = 0$, the exponential term of the function G_m is equal to one and convergence also becomes very slow. Another disadvantage of the Green's function G_m is that the singularity as $y \to y_S$ is not explicit.

The influence coefficients of elements on the interfaces of regions of constant depth and containing acoustic sources are calculated, for regular integration ($\mathbf{S}_p \neq \mathbf{X}_q$), as:

$$H_{pq} = \frac{L_q}{2}\int_{-1}^{+1} \frac{\partial G_m(\mathbf{S}_p, \mathbf{X}_q)}{\partial n(\mathbf{X}_q)} d\eta \tag{30}$$

$$G_{pq} = \frac{L_q}{2}\int_{-1}^{+1} G_m(\mathbf{S}_p, \mathbf{X}_q)\, d\eta \tag{31}$$

and for singular integration ($\mathbf{S}_p = \mathbf{X}_p$) as:

$$H_{pp} = \frac{L_p}{2}\int_{-1}^{+1} \frac{\partial G_B(\mathbf{S}_p, \mathbf{X}_p)}{\partial n(\mathbf{X}_p)} d\eta + \frac{1}{2} \tag{32}$$

$$G_{pp} = \frac{L_p}{2}\int_{-1}^{+1} G_F(\mathbf{S}_p, \mathbf{X}_p)\, d\eta \tag{33}$$

$$b_p = \sum_{\alpha=1}^{Nes} B_\alpha G_m(\mathbf{E}_\alpha, \mathbf{S}_p) \tag{34}$$

For regions with irregular bottom, the influence coefficients and contribution of the acoustic sources are obtained as

$$H_{pq} = \frac{L_q}{2}\int_{-1}^{+1} \frac{\partial G_f}{\partial n}(\mathbf{S}_p, \mathbf{X}_q)\, d\eta + \frac{1}{2}\delta_{pq} \tag{35}$$

$$G_{pq} = \frac{L_q}{2}\int_{-1}^{+1} G_f(\mathbf{S}_p, \mathbf{X}_q)\, d\eta \tag{36}$$

$$b_p = \sum_{\alpha=1}^{Nes} B_\alpha G_f(\mathbf{E}_\alpha, \mathbf{S}_p) \tag{37}$$

where δ_{pq} is the Kronecker delta.

The integrals in Eq. (32) and (33) are computed numerically using Gaussian quadrature for either the complete series or term by term. In the first case, the number of Gauss points must be the same for terms with small and large r, increasing the computer time. A term by term integration with different numbers of Gauss points has been used. In addition, the asymptotic form of the Hankel function is employed to integrate terms with source point reflection far from the bottom and free surface.

4 Applications

All the examples analysed here simulate the propagation of acoustic waves in shallow water due to an acoustic source of unit magnitude, with the sound velocity c taken to be $1500m/s$.

4.1 Region containing a vertical step-up

The first example, shown in Fig. 4, deals with a region containing a vertical step-up located at $20m$ from the origin. The deeper and shallower ends are equal to $1.0m$ and $0.5m$, respectively. The frequency f is taken to be $1000Hz$ and the acoustic source is located at $x_E = 0.0m$ and $y_E = 0.5m$.

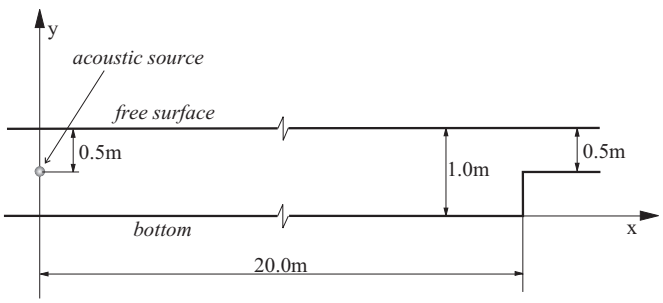

Figure 4 : Geometry for vertical step-up on the seabed ($h = 1.0m$)

The boundary element discretisations are depicted in Fig. 5. In type (a), only Γ_{12} and the step-up Γ_1 are discretised, each with 96 constant elements of graded length, concentrated close to point 2 (*vv192*). In type (b), the interface Γ_{12} was moved to a vertical line $5.0m$ from the step and the external boundary Γ_1 was extended along the bottom of the shallower depth. The interface and vertical line of the boundary are discretised as in type (a), while the horizontal line is discretised with 192 constant elements of graded length, concentrated close to points 2 and 3 (*vh384*).

In order to assess the accuracy of the results, a comparison was made with a solution obtained using an alternative BEM formulation in which the bottom boundary is fully discretised with 8088 graded elements, but the free surface is eliminated using a single image source. The infinite bottom boundary was truncated at the distances $-780.5m$ and $+820.5m$. It was

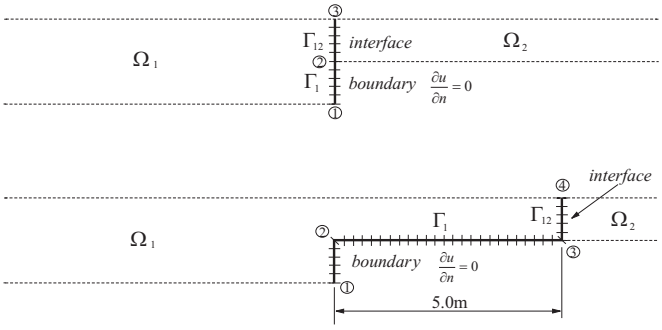

Figure 5 : Discretisation of the problem using graded elements, (a) only along the vertical line (vv), (b) along vertical and horizontal lines (vh)

found by trial and error that increasing these truncation distances produced very little difference in the solution.

Fig. 6 presents the velocity potential at internal and nodal points along the vertical line $x = 20m$, for different types of discretisation. Fig. 7 shows the velocity potential either on the interface or at internal points along the vertical line $x = 25m$. It can be seen that the results depict a good agreement for all discretisations, confirming that the use of subregions is appropriate for this type of problem.

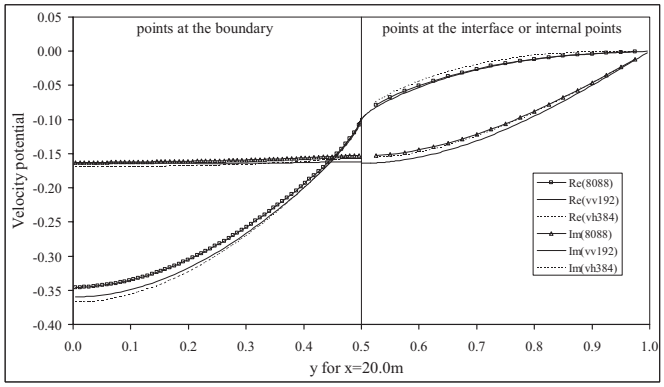

Figure 6 : Velocity potential at points along the vertical line $x = 20.0m$

4.2 Smooth deformations on the seabed

In the next two examples, the frequency f was varied from $15Hz$ to $150Hz$ in increments of $2.5Hz$ to observe the behaviour of the velocity potential along the bottom and at selected horizontal and vertical lines, for a range of frequencies.

The deformed bottom surface is described by the following sinusoidal function $f(x)$:

$$f(x) = \frac{a_d}{2}\left\{1+\cos\left[\frac{2\pi\,(x-x_0)}{w_d}\right]\right\}$$

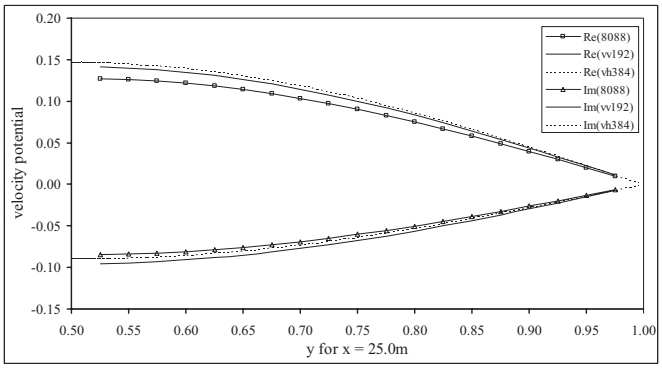

Figure 7 : Velocity potential at points along the vertical line $x = 25.0m$

$$|x-x_0| < w_d/2 \tag{38}$$

where a_d and w_d are the height and total width of the deformation, and x_0 is the algebraic value of the distance from the y-axis to the peak of the deformation.

4.2.1 A simple cosine bell on the bottom

The application is a coastal area with a simple cosine bell deformation at the bottom, shown in Fig. 8. The acoustic source is located at the position (0.0m, 150.0m), directly over the center of the peak. The height a_d and width w_d of the deformation are taken to be $50.0m$ and $100.0m$, respectively. Only the deformation was discretised, using more than 20 elements per wavelength for all frequencies.

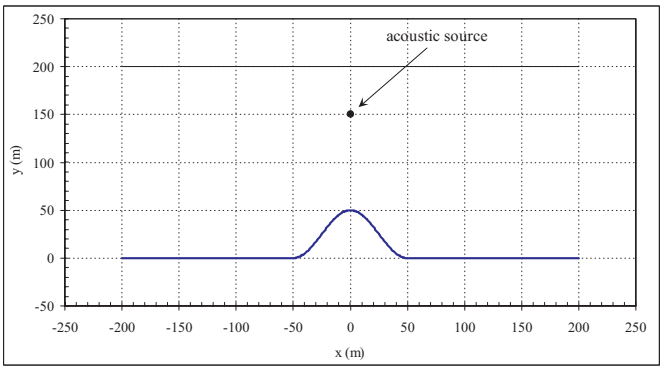

Figure 8 : Geometry of a coastal area with a simple cosine bell

The amplitude of the velocity potential along the cosine bell deformation is presented in Fig. 9, for five selected frequencies. The resulting velocity potential field is seen to be symmetric about the peak, as would be expected for this centered source, and to become more complex as the frequency increases. It can be noticed that small perturbations in the results

appear, at the ends of the cosine bell, for the highest frequencies of $f = 100Hz$ and $f = 150Hz$.

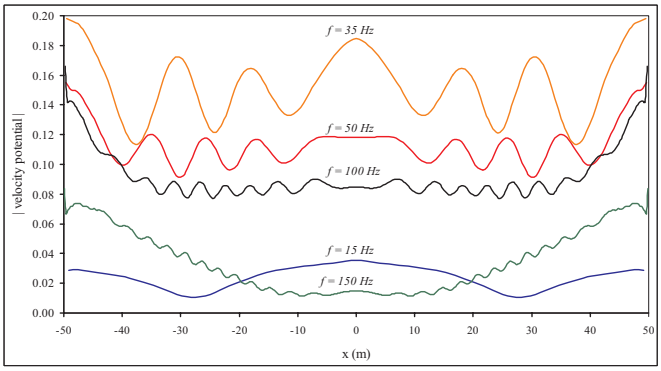

Figure 9 : Amplitude of the velocity potential along the cosine bell deformation

Fig. 10 depicts the variation of the velocity potential along the vertical line $x = 0.0m$, for the range of frequencies. It can be seen that the number of propagating modes increases as the frequency increases.

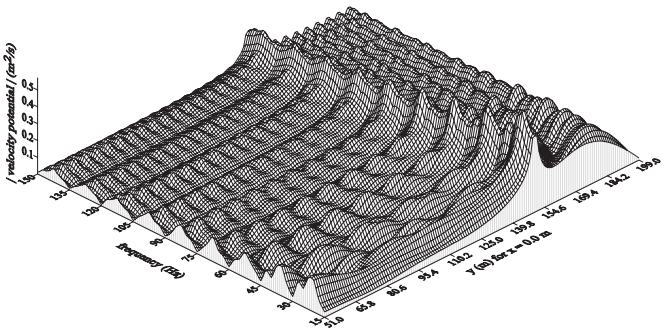

Figure 10 : Amplitude of the velocity potential along the vertical line $x = 0.0m$, for a range of frequencies from $15Hz$ to $150Hz$

The variation of the velocity potential along the horizontal line $y = 150.0m$ is presented in Fig. 11. The presence of the source located at $x = 0.0m$ can clearly be observed in the figure.

4.2.2 Idealised seabed close to shore

An idealised region close to shore, containing two sloping surfaces and a cosine bell deformation on the seabed, as depicted in Fig. 12, was analysed in order to observe the behaviour of the velocity potential with depth and range. The deeper and shallower regions are equal to $100.0m$ and $50.0m$, respectively. The acoustic source is located at $(-200.0m, 75.0m)$. Two subregions were employed to simulate this problem, with an interface at $x = 0.0m$. The height and width of the slopes and

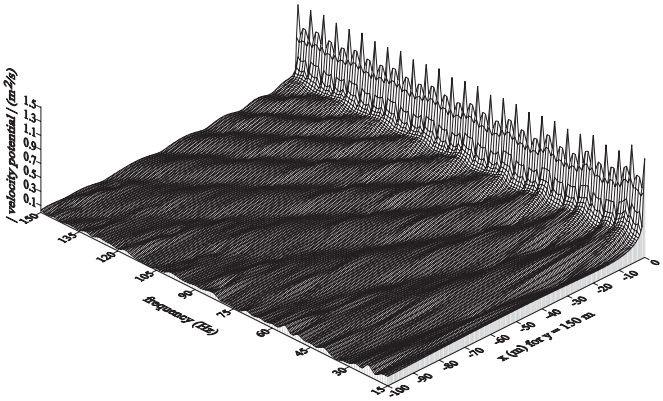

Figure 11 : Amplitude of the velocity potential along the horizontal line $y = 150.0m$, for a range of frequencies from $15Hz$ to $150Hz$

deformation are presented in Tab. 1. Notice that the sloping surfaces are half cosine bells, and their width in Tab. 1 are half the value of w_d in Eq (38).

Table 1: Height and width of slopes and deformation

	height (m)	width (m)
left slope	50	200
deformation	10	100
right slope	100	400

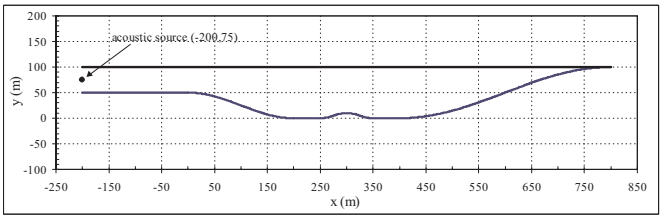

Figure 12 : Geometry for region containing two slopes and a deformation on the seabed close to shore

Fig. 13 and 14 present the amplitude of the velocity potential along two vertical lines at $x = -50.0m$ and $x = 300.0m$. Fig. 13 shows that, for the frequency of $15Hz$, only one propagating mode can be seen in the shallower region of depth $H = 50.0m$ while two propagating modes can clearly be seen in Fig. 14 for the deeper region of depth $H = 90.0m$. The number of propagating modes substantially increases with frequency for both the shallower and deeeper regions.

5 Conclusions

In this paper, we have presented a boundary element formulation for underwater acoustic wave propagation and scattering

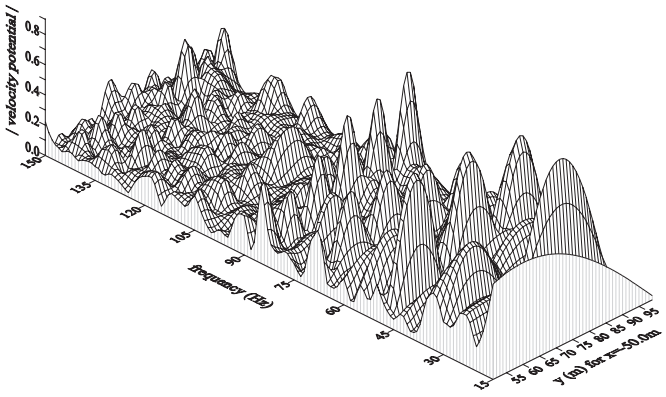

Figure 13 : Amplitude of the velocity potential along the vertical line $x = -50.0m$, for a range of frequencies from $15Hz$ to $150Hz$

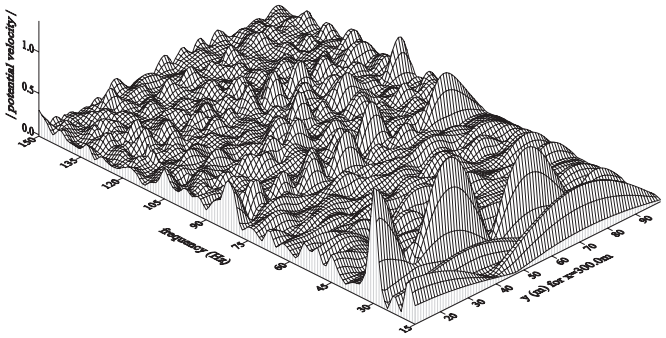

Figure 14 : Amplitude of the velocity potential along the vertical line $x = 300.0m$, for a range of frequencies from $15Hz$ to $150Hz$

by localised irregularities. Since the Green's functions adopted identically satisfy the boundary conditions at the free surface and horizontal seabeds, it is possible to use the subregions technique developed and validated here to simulate complex problems with bottom irregularities. By doing so, the boundary element discretisation is restricted to the localised irregularities and interfaces between regions of different depth.

Although the series (25) in terms of normal modes dramatically improves the speed of convergence, it is still necessary to improve the convergence of the infinite series when the source and field points are located along the same vertical line. Numerous techniques exist for accelerating slowly-convergent series, such as Euler's transformation for alternating series [Abramowitz and Stegun (1965)], Shanks transformation [Shanks (1955)], Wynn's algorithm [Wynn (1966)], Kummer's transformation [Linton (1998)] and Ewald's method [Linton (1998)], among others. The implementation and comparison of the efficiency of some of these techniques is presently under way.

Acknowledgement: The first author would like to thank CNPq, the Brazilian Research Council, for providing financial support to this research.

References

Abramowitz, M.; Stegun, I.A. (1965): *Handbook of Mathematical Functions*. Dover, New York.

Chen, G.; Zhou, J. (1992): *Boundary Element Methods*. Academic Press, London.

Dawson, T.W.; Fawcett, J.A. (1990): A boundary integral equation method for acoustic scattering in a waveguide with nonplanar surfaces. *J. Acoust. Soc. Amer.,* vol. 87, pp. 1110-1125.

Grilli, S.; Pedersen, T.; Stepanishen, P. (1998): A hybrid boundary element method for shallow water acoustic propagation over an irregular bottom. *Eng. Anal. Boundary Elements*, vol. 21, pp. 131-145.

Jensen, F. B.; Kuperman, W. A.; Porter, M. B.; Schmidt, H. (1994): *Computational Ocean Acoustics*. American Institute of Physics, Woodbury, NY.

Kinsler, L.E.; Frey, A.R.; Coppens, A.B; Sanders, J.V. (1982): *Fundamentals of Acoustics*. John Wiley, New York.

Lacerda, L.A. (1997): *Boundary Element Formulations for Outdoor Sound Propagation*. PhD Thesis, Department of Civil Engineering, COPPE / UFRJ, Brazil.

Linton, C.M. (1998): The Green's function for the two-dimensional Helmholtz equation in periodic domains. *J. Eng. Math.*, vol. 33, pp. 377-402.

Pedersen, T.K. (1996): *Modelling Shallow Water Acoustic Wave Propagation*. MSc Thesis, Department of Ocean Engineering, University of Rhode Island, USA.

Santiago, J.A.F.; Telles, J.C.F.; Valentim, V.A. (1999): An optimized block matrix manipulation for boundary elements with subregions. *Adv. Eng. Soft.*, vol. 30, pp. 701-713.

Santiago, J.A.F.; Wrobel, L.C. (1999a): Numerical modelling of the propagation of underwater acoustic waves. *15^{th} Brazilian Congress of Mechanical Engineering*, Águas de Lindóia, Brazil.

Santiago, J.A.F.; Wrobel, L.C. (1999b): 2D modelling of shallow water acoustic wave propagation using subregion techniques. *International Conference on Boundary Element Techniques*, Queen Mary and Westfield College, University of London, UK.

Shanks, D. (1955): Non-linear transformations of divergent and slowly-convergent sequences. *J. Math. Phys.*, vol. 34, pp.1-42.

Wynn, P. (1966): On the convergence and stability of the epsilon algorithm. *SIAM J. Numer. Anal.*, vol. 3, pp. 91-122.